An Algorithm to Determine the Spatial and Temporal Distributions of Sea Ice Leads in the Arctic

Grant number: NNX14AJ42G
Annual report for the time period 28 May 2016 – 27 May 2017

University of Wisconsin - Madison
Space Science and Engineering Center
Cooperative Institute for Meteorological Satellite Studies
1225 W. Dayton Street, Madison, WI

Investigators:

Steven A. Ackerman (PI)
Jay Hoffman
Jeffrey Key
Yinghui Liu

Table of Contents

Overview

We are developing a new algorithm, data product, and Algorithm Theoretical Basis Document (ATBD) to improve the monitoring of Arctic sea ice conditions: a sea ice lead-detection algorithm for the MODerate Resolution Imaging Spectrometer (MODIS) Imagers on Terra and Aqua. The ATBD will describe the algorithm, demonstrate applications, develop an initial data product release plan, and provide example data sets.

1. Introduction

Leads are elongated cracks in the sea ice cover. They form under stresses due to atmospheric winds and ocean currents (e.g., Smith et al., 1990). The open water refreezes as it is exposed to a cold atmosphere, so leads may contain unfrozen water or ice of varying thicknesses. They may be a few meters or a few kilometers in width, and may be tens of kilometers in length. In comparison to ice covered regions, leads provide a significant amount of heat and moisture to the Arctic atmosphere (e.g. Alam and Curry 1995, Maykut, 1987). While leads may occupy a relatively small area of pack ice (e.g. 1-2% of an area), the open waters provide a significant exchange of heat and moisture between the ocean and atmosphere, particularly during winter. They are also important for navigation and wildlife.

The long-term distribution of leads in sea ice and how these distributions might be changing is not well known. With the rapid thinning of the ice pack over the last decade, along with the reduction in sea ice area and the recent increase in sea ice velocity (e.g. Hakkinen et al., 2008), we hypothesize that we will see a change in the lead distributions and properties from earlier studies, and likely in the 13 year period of MODIS. Knowledge of this distribution of leads is important of climate and energy budget studies of the Arctic region.

Recent satellite observations show dramatic changes in the Arctic ice sheets, including a trend of shrinking sea ice extent and area over the last decade and a thinning of the sea ice. The ICESat and future ICESat-2 NASA missions contribute to these finding. The ICESat missions seek to determine inter-annual and long-term changes in polar ice-sheet volume to sufficient accuracy to assess their impact on global sea level (e.g. Zwally et al., 2002). The AMSR-E instrument on NASA's Aqua mission, and now AMSR2 on Japan's GCOM-W1 satellite, aid in the monitoring of sea ice extent and motion. Categorizing leads, including area coverage, frequencies, length and orientation, will contribute to these missions in the study of Arctic sea ice.

Leads impact climate in a number of ways. Leads have a lower albedo than the surrounding ice, and thus absorb more solar energy than surrounding ice. An increase in the ice leads can warm

water beneath the leads and increase the melting of the surround ice. When leads open, the warmer ocean water releases heat and moisture into the atmosphere, and impact the atmospheric structure and cloud properties above. Comparison of results from this proposal with trends in other Arctic sea ice properties (e.g. thickness, coverage, movement) will help understand the ice dynamics under changing environment conditions, and interactions of climate system components.

One of NASA's science objectives is to address the question: "*How and why are Earth's climate and the environment changing*?" This project addresses this question by characterizing the distribution of leads in the Arctic Ocean. Observations of sea ice lead characteristics need to be measured to understand changes in the sea ice and their response to atmospheric and oceanic forcing. Understanding these responses should ultimately enable more accurate climate predictions and characterizations of uncertainties. Recent observed declines in ice extent and area result from a warming of the atmosphere and ocean, which drives a decrease in ice thickness and perhaps an expansion of leads, even though there might be more ice production during winter as ice reforms in the leads. To fully understand this dynamic between the Arctic sea ice area and thickness, the number and area coverage of leads and atmosphere and ocean circulations, we need to measure the general distribution of leads and determine how this distribution has been changing. We begin this with the development of an algorithm to achieve those measurements.

2. Accomplishments

Our initial approach relied on the Key et al. (1993 and 1994) algorithm. Those studies applied the algorithm to locate leads then determine their length, width and orientation. While developed for LandSat, which has limited coverage of the polar ice caps, the methodology is portable to other optical sensors, such as AVHRR and the NASA MODIS imagers. AVHRR and MODIS have better spatial coverage and temporal coverage, but lack the spatial resolution of LandSat. Key et al. (1993) explored the sensitivity to lead detection using the AVHRR thermal imagery under various atmospheric conditions. Their results indicated that the limits of lead detection were a function of subpixel lead fraction and atmospheric optical depth, if suitable values of normalized contrast were used in the detection criteria.

The technical overview of the new approach adapted from Key et al. (1993 and 1994) requires the following steps:

- Access MODIS granules
- Stitch together the granules in an orbit that covers the arctic region
- Determine the fraction of cloud cover (from MOD35 and MYD35)
- Determine the fraction of ice coverage fraction in a pixel

- Identify objects where the ice fraction within the pixel is less than 95%
- Connect objects that are close (within a couple of pixels)
- Identify linear features using imaging analysis tools, such as Hough transform, Sobel filtering and connectivity.
- Determine lead properties (length, area, etc.)

Last year we developed the initial algorithm and applied the data to an extended period of MODIS data. Doing multiple years allows us to identify issues with the data and the algorithm. This past year we have explored and refined methods for connecting lead segments into a single lead, thus improving the detection. Improvement to the algorithm also included deep ocean waters, previously we were limited to depths of 500m or greater. This was an attempt to avoid shore leads in the algorithm, but analysis indicated too large an area as eliminated. We finalized version 3 of the algorithm, the flow chart is shown in Figure 1.

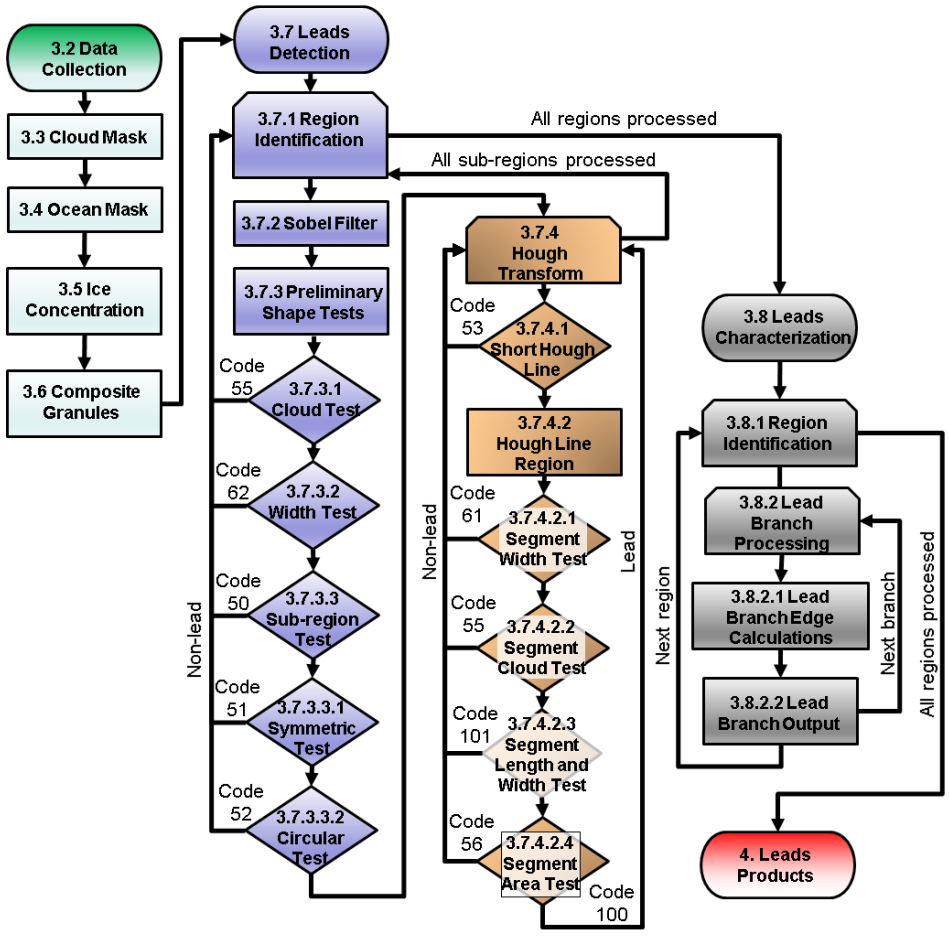

Figure 1 Leads algorithm flowchart.

Algorithm Application

The algorithm was applied to Aqua and Terra MODIS observations between 2004 and 2016. We are using this time to identify trends that may reflect issues or errors with the algorithm. Figure 2 shows the ratio of the lead area divided by the total regional area sampled (right figure) and the normalized areal cloud-free coverage (left figure) for the years 2003-2016. The decreasing trend in lead area appears correlated with the average trend in cloud clover. Decreasing cloud-free coverage means more cloud and a likelihood of reduced ability to detect the presence of a lead. However, there is no strong year-to-year correlation between the cloud-free region and lead areal covers. We continue to assess how cloud cover may impact the statistics of the algorithm results.

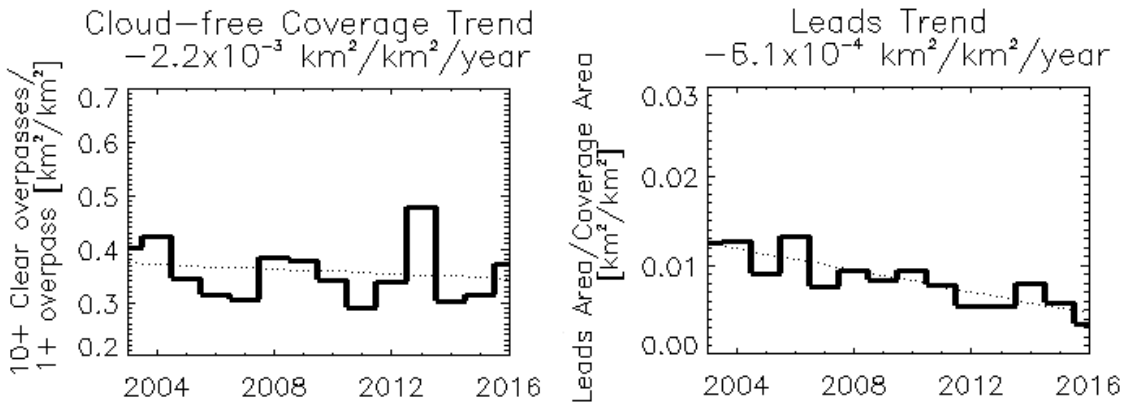

Figure 2 Number of cloud-free overpasses (left) and leads area coverage (right) over the Arctic Ocean for the years 2003 to 2016.

3. Milestones

The milestones achieved to date:

- Collected a 15-year (2003-2017) set of Arctic scenes of Aqua and Terra MODIS for processes of Level-1 data at 1 km resolution and corresponding cloud mask.
- Combined consecutive granules into a single swath over Arctic.
- Applied sea ice concentration, leveraging that being developed for GOES-R and JPSS algorithms.
- Developed and tested the lead detection algorithm.

- Applied the algorithm to MODIS (2003-2017) to try and identify algorithm issues
- Began writing ATBD

Coming year activities:

- Continue and complete testing of lead characterization algorithm.
- Assess performance of lead algorithm through comparison of lead from MODIS 1-km data with lead from higher spatial resolution data.
- Develop lead properties (e.g. area coverage, length, width, orientation) algorithm.
- Have ATBD reviewed and delivered.

4. Conference Presentations

Hoffman, J. P., S. A. Ackerman, Y. Liu, and J. R. Key, 2017: Satellite Detection of Arctic Sea Ice Leads, 2017: 97th Annual meeting of the American Meteorological Society, Seattle, WA, January 22 - 26

Hoffman, J., S. A Ackerman, Y. Liu, J. R. Key, 2016: Trends in Arctic Sea Ice Leads Detection. American Geophysical Union Fall meeting, San Francisco CA, December 12-16.

5. References and Citations

Ackerman, S. A., K. I. Strabala, W. P. Menzel, R. A. Frey, C. C. Moeller, and L. E. Gumley Discriminating Clear-sky from Clouds with MODIS, 1998: *J. Geo. Res*., **103** , D24, p. 32,141

Alam, A. and J. Curry, 1995: Lead-induced atmospheric circulations. *Jour Geo Res*, **100**, C3, 4643-4651.

Appel I., and J. A. Kenneth, 2002: Fresh water ice Visible/Infrared Imager/Radiometer Suite algorithm theoretical basis document, Version 5. SBRS document #: Y2404.

Frey, R. A., S. A. Ackerman, Y. Liu, K. I. Strabala, H. Zhang, J. Key and X. Wang, 2008: Cloud Detection with MODIS, Part I: Recent Improvements in the MODIS Cloud Mask, *JTECH* **25**, 1057-1072.

Hakkinen, S., A. Proshutinsky, and I. Ashik, 2008: Sea ice drift in the Arctic since the 1950s, *Geophys. Res. Lett.*, **35**, L19704, doi:10.1029/2008GL034791, 184

Hall D.K., G.A. Riggs, and V.V. Salomonson, 2001: Algorithm theoretical basis document for the MODIS snow and sea ice mapping algorithms.

Hall D.K., G.A. Riggs, and V.V. Salomonson, 2006: MODIS sea ice products user guide to collection 5.

Key, J., J.A. Maslanik, and E. Ellefsen, 1994: The effects of sensor field-of-view on the geometrical characteristics of sea ice leads and implications for large-area heat flux estimates. *Remote Sensing Environ*., **48**(3), 347-357.

Key, J., R. Stone, J. Maslanik, and E. Ellefsen, 1993: The detectability of sea ice leads in satellite data as a function of atmospheric conditions and measurement scale. *Annals Glaciol*., **17**, 227-232.

Liu Y., and J.R. Key, 2010: Algorithm theoretical basis document for ABI ice cover and concentration. NOAA NESDIS center for satellite applications and research.

Maykut, G. A., 1978: Energy exchange over young sea ice in the central Arctic. *J. Geophys. Res*., **83** (C7), 3646-3658.

Miles, M. W., and R. G. Barry, 1998: A 5-year satellite climatology of winter sea ice leads in the western *Arctic, J. Geophys. Res*., **103**(C10), 21,723–21,734, doi:10.1029/98JC01997.

Murray, R.J., and I. Simmonds, 1995: Responses of climate and cyclones to reductions in Arctic winter sea ice. *J. Geophys. Res*., **100**, 4791-4806.

Smith, S. D., R. D. Muench and C. H. Pease, 1990: Polynyas and leads: An overview of physical processes and environment, J*. Geophys. Res*. **95**, 9461-9470.

Zwally, J., et al., 2002: ICESat's laser measurements of polar ice, atmosphere, ocean and land, *J. Geodyn*., **34**, 405–445.

Budget Justification

Award NNX14AJ42G

An Algorithm to Determine the Spatial and Temporal Distributions of Sea Ice Leads in the Arctic

5/28/2017-5/27/2019

Budget

Part I: Budget Narrative

This project got started late as the initial programmer left the university before the project got underway.

For the remainder of the award NNX14AJ42G we submit our budget justification for the remaining $141,869 to fund the University of Wisconsin's portion of the research outlined in the project narrative. This amount includes the remaining $23,507 of current funding, combined with the anticipated Year 2 funding of $118,647. Explanations of the budget information are given directly below. The costs to conduct the activities described in this proposal are summarized in the budget pages provided. Cost estimates in these budget pages are based on historical events and experience.

Personnel

The following individuals have been identified as key personnel to this proposal:

Steve Ackerman, PI 60 hours

Yinghui Liu, Co-I 45 hours

Time quoted for key personnel is the total amount of anticipated sponsor paid effort required to complete the proposed effort over the life of the project, including during periods of no cost

extension. Fulfillment of the effort commitment will be defined as a total for the entire project period. We cannot guarantee effort for key personnel commitments per budget period given the uncertain volatile nature of research and funding availability. Funding reductions will result in a scaled back effort; the project narrative, the budget, and key personnel obligations will all be reduced in the same manner (i.e. if the funding is cut 25%, we will cut 25% of the project narrative and 25% of the labor and cost involved) unless otherwise negotiated.

This section identifies the staff required, their effort (hours needed), and salary information. To calculate hourly rates for salaried employee, the formula is Total Salary divided by billable hours. Hourly rates are calculated using a base of 1350 hours per year for Faculty and 1,791 billable hours per year for Academic Staff. Undergraduates are paid on an hourly basis, so no computation is required. Vacation, holiday and sick leave time is not charged directly to the projects. For budgets with duration greater than one year, we use a 3% inflation factor to labor rates to account for cost of living adjustment. We estimate an approximate total effort as follows:

Table of Personnel and Work Effort

			5/28/2017-5/27/2018	
Name	Title	Classification	Hours	% Effort
Ackerman, Steven	Principal Investigator	Faculty	60	3%
Liu, Yinghui	Co-Investigator	Academic Staff	45	3%
Hoffman, Jay	Researcher	Academic Staff	1603	90%

Fringe Benefits

Fringe rates are dependent on employee classification (which is listed under the Personnel section).

For a detailed rate breakdown, please visit: https://www.rsp.wisc.edu/chap4/rn/rn17-1.html

Travel

Travel costs are for UW-Madison staff to attend meetings, workshops and professional conferences. The travel budgets in the proposal are based on recent history regarding the amount of travel needed to conduct the research project, interact with collaborators, and present the results. The SSEC travel office monitors current airfares, hotel costs, car rentals,

taxi fares, etc and provides estimates for travel costs for frequent meeting sites. The UW-Madison, in accordance with state law, reimburses per diem travel costs for hotel and meal expenses. All travel must be approved by the SSEC administration. Travel costs are reviewed by the SSEC travel office and one of the SSEC Executive Directors. For this proposal one trip to the DC area for science team meeting and dissemination of results is budgeted. Total travel cost budgeted for the remainder of this project is $1,699.

1 Trips for 1 person / 4 days / DC, science meeting				
	fares		subtotal	
Airfare	1	500	500	
	# days	cost / day		
Hotel	3	289	867	
Meals	3.5	69	241.5	
Local Transportation	4	10	40	
Airport transportation - Madison	2	25	50	
				1,699

Materials & Supplies

We are requesting funding in total of $ 102 for nominal Materials and Supplies. These items are required to support the research infrastructure of a particular project. They include items such as data disks and tape cartridges, small computer peripherals, off the shelf computer software such as compilers, computer maintenance licensing agreements, conference registration and abstracts, and in-house publishing. Costs are based on current estimates and recent purchases with our contracted providers.

Other

Publications costs are based on a $145 per page charge, which is the standard rate for refereed journal publications from the American Meteorological Society. Publication size is based on historical evidence from previous projects and expected publications from this project in the coming year. For this project, we anticipate one publication for a total of $2,175.

Indirect Cost

Currently at 53%, the indirect cost rate is directly negotiated with the U.S. government and is charged to all budget items except capital equipment purchases over $5,000, participant support costs, and student tuition remission, which are free of overhead. The first $25,000 of a subcontract award is subject to university overhead, any award above $25,000 is free of overhead. A copy of the rate agreement can be found at:
https://www.rsp.wisc.edu/rates/rates.pdf

Part II: Budget Details

Projected Budget Summary

5/28/2017-5/27/2018

I.	Labor and Fringe Benefits	Hours	Rate	Salary	Fringe %	Fringe	Cost	Totals
	PI - Steve Ackerman	65	124.79	$ 8,112	35.0%	$ 2,840	$ 10,952	
	CoI - Yinghui Liu	45	45.23	$ 2,035	35.0%	$ 712	$ 2,747	
	Researcher - Jay Hoffman	1603	34.68	$ 55,592	35.0%	$ 19,458	$ 75,050	
	Subtotal							$88,749
II.	Materials and Supplies							102
III.	Travel							
	a) 1 Trips for 1 person / 4 days / DC, science meeting							1,699
IV.	Publication 15 pages @ $145 each page							2,175
V.	University Indirect Cost at 53%							49,144
	TOTAL							$141,869

Funds Remaining

5/28/2017-5/27/2018

I.	Labor and Fringe Benefits	Hours	Rate	Salary	Fringe %	Fringe	Cost	Totals
	PI - Steve Ackerman	20	124.79	$ 2,496	35.0%	$ 874	$ 3,370	
	CoI - Yinghui Liu	10	45.23	$ 452	35.0%	$ 158	$ 610	
	Researcher	242	34.68	$ 8,393	35.0%	$ 2,938	$ 11,331	
	Subtotal							$15,311
II.	Materials and Supplies							53
III.	Travel - none							0
IV.	Publication 15 pages @ $145 each page							0
V.	University Indirect Cost at 53%							8,143
	TOTAL							$23,507

Year 2 Anticipated Funding									
		5/28/2017-5/27/2018							
I.		Labor and Fringe Benefits	Hours	Rate	Salary	Fringe %	Fringe	Cost	Totals
		PI - Steve Ackerman	45	124.79	$ 5,616	35.0%	$ 1,966	$ 7,582	
		CoI - Yinghui Liu	35	45.23	$ 1,583	35.0%	$ 554	$ 2,137	
		Researcher	1361	34.68	$ 47,199	35.0%	$ 16,520	$ 63,719	
		Subtotal							$73,438
II.		Materials and Supplies							49
III.		Travel							
	a)	1 Trips for 1 person / 4 days / DC, science meeting							1,699
IV.		Publication 15 pages @ $145 each page							2,175
V.		University Indirect Cost at 53%							41,001
		TOTAL							$118,362

Appendix A

CIMSS Algorithm to Determine the Spatial and Temporal Distributions of

Sea-ice Leads in the Arctic Algorithm Theoretical Basis Document

University of Wisconsin - Madison

Space Science and Engineering Center

Cooperative Institute for Meteorological Satellite Studies

Jay Hoffman, Steven A. Ackerman, Yinghui Liu, Jeffrey Key

Version 1.0

Table of Contents

LIST OF FIGURES

LIST OF TABLES

LIST OF EQUATIONS

ABSTRACT

This ATBD presents a new methodology to detect and characterize sea ice leads with optical (visible, infrared) satellite data. Using reflective and emissive channels, ice concentration is derived in cloud-free regions and used to create a mask of potential lead pixels. The algorithm then identifies and characterizes leads with a combination of image processing techniques that examine shape characteristics. Data from the Moderate Resolution Imaging Spectroradiometer (MODIS) are used to assess the spatial and temporal distributions of Arctic sea ice leads and their changes since 2002. Sea ice leads (fractures) play a critical role in the exchange of mass and energy between the ocean and atmosphere in the polar regions, particularly in the Arctic. Given the rapid thinning and loss of Arctic sea ice over the last few decades, changes in the distribution of leads can be expected in response. Leads are largely wind driven, so their distributions will also be affected by the changes in atmospheric circulation that have occurred. From a climate perspective, this new product can be used to identify trends in lead characteristics (width, orientation, and spatial distribution). From an operational perspective, knowledge of lead characteristics can aid in navigation, with direct benefits to security, subsistence hunting, and recreation.

1. Introduction

Leads are elongated cracks in the sea ice cover. They form under stresses due to atmospheric winds and ocean currents (e.g., Smith et al., 1990). The open water refreezes as it is exposed to a cold atmosphere, so leads may contain unfrozen water or ice of varying thicknesses. They may be a few meters or a few kilometers in width, and may be tens of kilometers in length. In comparison to ice covered regions, leads provide a significant amount of heat and moisture to the Arctic atmosphere (e.g. Alam and Curry 1995, Maykut, 1987). While leads may occupy a relatively small area of pack ice (e.g. 1-2% of an area), the open waters provide a significant exchange of heat and moisture between the ocean and atmosphere, particularly during winter. They are also important for navigation and wildlife.

The long-term distribution of leads in sea ice and how these distributions might be changing is not well known. With the rapid thinning of the ice pack over the last decade, along with the reduction in sea ice area and the recent increase in sea ice velocity (e.g. Hakkinen et al., 2008), we hypothesize that we will see a change in the lead distributions and properties from earlier studies, and likely in the 13 year period of MODIS. Knowledge of this distribution of leads is important of climate and energy budget studies of the Arctic region.

Recent satellite observations show dramatic changes in the Arctic ice sheets, including a trend of shrinking sea ice extent and area over the last decade and a thinning of the sea ice. The ICESat and future ICESat-2 NASA missions contribute to these finding. The ICESat missions seek to determine inter-annual and long-term changes in polar ice-sheet volume to sufficient accuracy to assess their impact on global sea level (e.g. Zwally et al., 2002). The AMSR-E instrument on NASA's Aqua mission, and now AMSR2 on Japan's GCOM-W1 satellite, aid in the monitoring of sea ice extent and motion. Categorizing leads, including area coverage, frequencies, length and orientation, will contribute to these missions in the study of Arctic sea ice.

Leads impact climate in a number of ways. Leads have a lower albedo than the surrounding ice, and thus absorb more solar energy than surrounding ice. An increase in the ice leads can warm water beneath the leads and increase the melting of the surround ice. When leads open, the warmer ocean water releases heat and moisture into the atmosphere, and impact the atmospheric structure and cloud properties above. Comparison of results from this proposal with trends in other Arctic sea ice properties (e.g. thickness, coverage, movement) will help understand the ice dynamics under changing environment conditions, and interactions of climate system components.

One of NASA's science objectives is to address the question: "How and why are Earth's climate and the environment changing?" This project addresses this question by characterizing the distribution of leads in the Arctic Ocean. Observations of sea ice lead characteristics need to be

measured to understand changes in the sea ice and their response to atmospheric and oceanic forcing. Understanding these responses should ultimately enable more accurate climate predictions and characterizations of uncertainties. Recent observed declines in ice extent and area result from a warming of the atmosphere and ocean, which drives a decrease in ice thickness and perhaps an expansion of leads, even though there might be more ice production during winter as ice reforms in the leads. To fully understand this dynamic between the Arctic sea ice area and thickness, the number and area coverage of leads and atmosphere and ocean circulations, we need to measure the general distribution of leads and determine how this distribution has been changing. We begin this with the development of an algorithm to achieve those measurements.

1.1. Overview

This ATBD describes the algorithm, demonstrates applications, and provide example data sets.

1.2. Algorithm History

Our initial approach relied on the Key et al. (1993 and 1994) algorithm. Those studies applied the algorithm to locate leads then determine their length, width and orientation. While developed for LandSat, which has limited coverage of the polar ice caps, the methodology is portable to other optical sensors, such as AVHRR and the NASA MODIS imagers. AVHRR and MODIS have better spatial coverage and temporal coverage, but lack the spatial resolution of LandSat. Key et al. (1993) explored the sensitivity to lead detection using the AVHRR thermal imagery under various atmospheric conditions. Their results indicated that the limits of lead detection were a function of subpixel lead fraction and atmospheric optical depth, if suitable values of normalized contrast were used in the detection criteria.

2. Instrument Description

This leads detection product uses the MODIS instrument onboard the Aqua and Terra satellite platforms.

3. Algorithm Description

The algorithm is based on the foundation the Key et al. (1993 and 1994) algorithm. Those studies applied the algorithm to locate leads then determine their length, width and orientation. The algorithm requires the MODIS Cloud Mask and Ocean Mask. Ice concentration is calculated and used to form a daily composite from which image analysis is used to detect and then characterize leads.

3.1. Algorithm Overview

The Aqua and Terra MODIS granules north of 66.5N are collected and remapped to a 1 km grid using a nearest neighbor approach. The leads detection algorithm next determines cloud-free

scenes, and if a pixel over deep ocean water surface is ice or open water. Cloud screening is done using the MODIS cloud mask (MxD35) (Ackerman et al. 1998 and Frey et al. 2008). Ice or snow-covered ice surfaces have high reflectance in the visible channels, very low reflectance in short-wavelength infrared channels, and lower surface temperature than open water and leads. During the day (solar zenith angle less than 85 degrees), a pixel is identified as potentially ice if the Normalized Difference Snow Index (NDSI) and the reflectance in a visible channel are both larger than preset thresholds (Hall et al. 2001, 2006), and if the surface temperature is lower than a preset thresholds. During the nighttime (solar zenith angle greater than or equal to 85 degrees), a pixel is identified as possible ice if the surface temperature is lower than some threshold. Ice concentration at each gridpoint/pixel is then calculated using tie-point algorithm in which a representative reflectance (daytime) or surface temperature (nighttime) of 100% ice covered surface is determined in a search window centered that gridpoint/pixel (Appel and Kenneth 2002, Liu and Key 2010). Under certain conditions where a single ice type appears in a search window with certain shape and size, surface reflectance or temperature of the pure ice is homogeneous and different from open water. Changes in surface reflectance/temperature at the pixel level are mainly due to different ice concentration, which is the fraction of the area (i.e., a pixel) covered by ice.

A daily composite of each overpass is derived in the 1 km grid where the composite is a count of the number of overpasses where sea ice concentration is below the threshold of 95%. From the daily composite leads are identified using a number of image processing techniques. Finally leads characteristics are derived from the subset of locations that have passed the initial leads detection tests.

3.2. Data Collection

Collect all Aqua and Terra overpasses from January through April where at least half of the granule is north of 66.5^{o} latitude.

3.3. Cloud Mask

Cloud screening is done using the MODIS cloud mask (MxD35) (Ackerman et al. 1998 and Frey et al. 2008). Cloudy is defined as confident cloudy and probably cloudy; clear is defined as confident clear and probably clear.

3.4. Ocean Mask

Leads detection are limited to ocean water deeper than 500m. This is done to prevent false leads detections along the ice edge.

3.5. Ice Concentration

In a search window with a size of 30 × 30 pixel, the ice reflectance/temperature probability density function (PDF) is calculated using all possible ice pixels detected in the first step. The ice reflectance/temperature tie point is chosen as the reflectance/temperature with the maximum probability density in the smoothed PDF. The open water reflectance/temperature tie point is parameterized based on solar zenith angle and salinity. Then, ice concentration for a pixel (F_p) inside the search window can be calculated by

$$(1)\ F_p = (B_p - B_{water}) / (B_{ice} - B_{water})$$

Where B_{water} is the reflectance/temperature of pure water pixels, B_{ice} is the reflectance/temperature of pure ice pixels; B_p is the observed reflectance/temperature of the pixel.

The foundation of the lead detection is based in ice concentration. A potential lead is defined as a location with an ice concentration between 0%-95%. A primary component of the leads detection algorithm is an image analysis algorithm that identifies regions of connected points as objects - in this case each connected region is a potential lead. The algorithm continues until all potential lead regions have been processed. The algorithm chooses the largest remaining potential lead region as the starting point for a processing segment.

Once the largest region is identified, a preliminary width test is run. An appropriate width is calculated as the quotient of the area of the potential lead points within the region is divided by the length of the diagonal line defined by the length of a rectangle box that encompasses the region. If the width is greater than 60 km, the region is identified as open water and no further processing is needed for the region. Otherwise, the leads detection algorithm will define a processing segment around the region of interest. The domain processing is more efficient when it processes medium sized segments that are neither too large (large regions execute too slowly) nor too small (processing numerous small segments is also computationally slow), so the horizontal and vertical segment span is defined as the greater of 750km or the span of the region spans. To avoid “breaking” a lead segment across processing segments, any potential lead that falls on the boundary of a processing segment will be excluded from the current processing segment (and remain to be processed in a later segment). A daily aggregate mask of lead frequency is derived from all MODIS (AQUA and TERRA) overpasses for each day (see Figure 3.5 for an example).

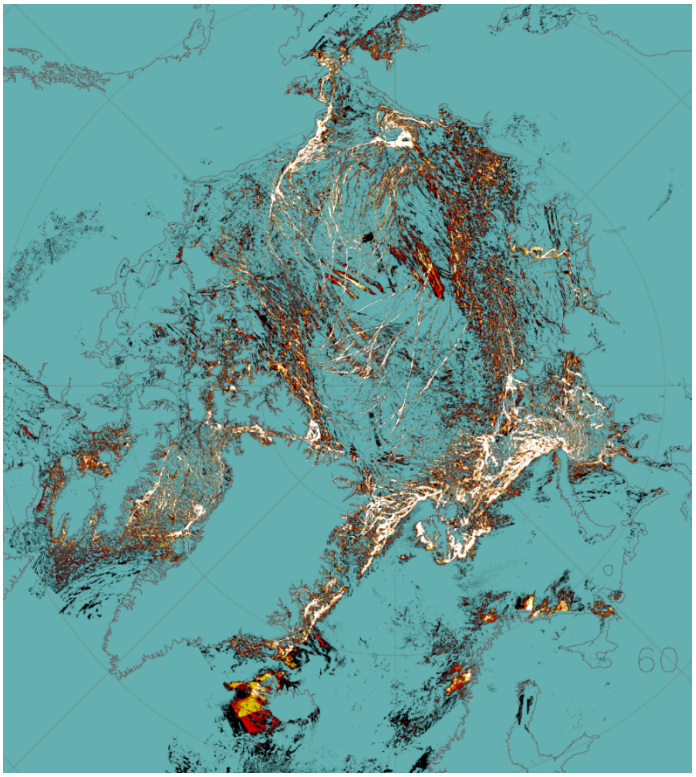

Figure 3.5. Lead frequency map from all MODIS overpasses in a day. This is a daily composite of those pixels with ice concentration between 0-95%. In this images, teal indicates no pixels throughout the day meet the conditions, black indicate only 1 pixel during the day met the ice concentration threshold, red indicates twice, yellow three times and white are those pixels that met the ice concentration threshold 4 or more times during the day.

3.6. Compositing Granules

After calculating sea ice concentration for each MODIS overpass, daily composite image is generated. Using the same 1 km grid as the sea ice concentration, a composite mask is generated as a count of the number of overpasses where sea ice concentration is below the threshold of 95%. In addition to the sea ice concentration composite count, a composite of the number of cloudy and total overpasses each location – these counts will help in later steps to establish detection confidence. The most confident leads detection occurs when the sea ice concentration threshold passes more than once and there are ten or more cloud-free overpasses within a day.

3.7. Leads Detection

The main leads detection algorithm begins by defining potential leads as any $1km^2$ grid point from the daily composite mask where the at least one overpass had sea ice concentration less than the threshold of 95%.

3.7.1. Region Identification

The first step in the image processing utilizes the IDL label_region function. From the mask of all points where the ice concentration is met one or more times, the IDL function assigns a unique region number for every object in the mask – where an object is defined as a group of one or more connected pixels. Once the regions numbers are defined, the processing begins to loop through the image until all regions greater than 2 pixels in area have been processed (regions with only one or two points are rejected for being too small). The processing loop begins by selecting the largest remaining object, a search window is defined around the largest remaining object until the selection window is 750km by 750km. The leads detection algorithm will process all potential leads within the selection window except for any potential leads that occur along or spans across the boundary of the selection window (these boundary regions are ignored temporarily and will be processed in a later loop iteration). The algorithm will continue to process the domain until all potential lead objects have been processed. The end result will is a binary raster mask that records a the processing code for each location and a text log file (described in 3.7.4.2).

3.7.2. Sobel Filter

For each selection windows the leads algorithm performs the following steps. First, a Sobel image filter is applied to the mask of the potential leads. This image filter helps to identify and connect linear features that might not be continuous in the native mask. This helps identify leads that may have sub-resolution elements along their path. The label_region function is used again, this time to define unique region numbers for each connected object in the Sobel filter mask. The processing logic starts with the largest Sobel filter mask region object and continues until all objects have been processed.

3.7.3. Preliminary Shape Tests

To help improve processing speed, some preliminary tests are executed to exclude some objects based on shape. These tests are done because the Hough Transform that will be described in section 3.7.4 is competitively expensive, so some quick tests are used to reduce the number of times the Hough Transform is called.

3.7.3.1. Cloud Test

The first test is to exclude regions with too few repeat detections of a potential lead within the day; if more than 90% of the potential lead object area was observed two or fewer times within a day, the region is flagged (code 55) and no further processing is done. This test removes features that are most likely cloud contaminated (cloud cover may have limited the number of sea ice concentration observations or else the cloud mask may have omission errors in a small number of overpasses that may result in false ice concentration derivation).

3.7.3.2. Width Test

Next, another test is run to test the approximate width of the region. The region area must be greater than 3 pixels (or else it will fail to have a valid line segment); the object area is divided by the length of the diagonal line that connects the opposing corners of a rectangle that encompass the region. Any region with an approximate width of greater than 60 km is flagged (code 62) as a non-lead feature.

3.7.3.3. Sub-region Tests

If a potential lead has passed the preliminary screening, then all remaining objects with an area greater than 3 points are subjected to more testing. First, the original mask is compared against the Sobel filtered mask to count the number of disconnected objects in the original mask that correspond to the single potential lead object region from the Sobel filter. A code non-lead flag (code 50) is assigned if an object has more than 1 sub-region, more than half of the object area is made up of sub-regions of less than 5 km^2, and there are less than five but more than two large (area greater than or equal to 5 km^2) sub-regions.

3.7.3.3.1. Symmetric Test

After testing for too many disconnected sub-regions, the next test is to test the object symmetry. To do this, a box is defined around the potential lead object and if the object area in each of the four quadrants is within +/-5% of 25% then the object is classified (code 51) as too symmetric and therefore not a lead.

3.7.3.3.2. Circular Test

Similarly, if too much of an object area falls within a circle drawn over the object, it is rejected as being too circular. The circle is defined at the center of the object with a radius of half of the distance spanned in the x and y directions. And, if more than half of the object points are within 1.5km of the edge of the circle, then the object is too circular and rejected (code 52).

3.7.4. Hough Transform

If a potential lead object has passed the preliminary shape tests described in section 3.7.3, the next test is to apply a Hough Transform to identify the longest linear feature within the region of interest.

3.7.4.1. Short Hough Line

If the Hough line has less than or equal to 3 points the region is classified as a non-lead (code 53) because the Hough line is too short.

3.7.4.2. Hough Line Region

If the Hough line is longer than 3 points, then calculate the length of the longest continuous line segment from the subset of points common between the Hough line and potential lead region. Then, define a region from the longest line segment find all of the potential lead points that are connected continuously with the line segment. This newly defined region is the sub-region that will be tested as the potential lead region. Calculate the area and length of the longest line segment within the sub-region – as it may be longer than the length the Hough line segment. If the sub-region area is greater than 2 points then there a few final tests to classify the region as a lead or non-lead. First, a lead code (code 100) is assigned to the output mask to all points that have made it this far in the processing. Some final test are only applied that could potentially change the mask code. Processing is done to only the largest remaining lead sub-region and regardless of the outcome of the tests, the rest of the potential lead object is processed until no more valid Hough line segment regions are found. After all of the tests described in this section, the results are written to a log file for decoding purposes. The output includes an identifier for the region number and the sub-region number, the start and end x and y coordinates as well as the latitude and longitude, the great circle object length, width, area, Hough line segment length, and the processing code. The text product for users will be generated in in the characterization process described in section 3.8.

3.7.4.2.1. Segment Width Test

There is a set of two criteria to reject a sub-region of a potential lead as being too wide. First, is the width test – or region area defined in section 3.7.4.2 divided by length – is greater than 25 km^2. And second, if the ratio of sub-region area divided by the product of the span in the x multiplied by the span in the y direction is greater 1/5. If both conditions are true the sub-region is flagged (code 61) as being too wide.

3.7.4.2.2. Segment Cloud Test

Similar the test in section 3.7.3.1, a cloud test is performed on the Hough line segment object. If more than 90% of the sub-region area was detected in less than or equal to two overpasses, then the sub-region is flagged (code 55) and rejected as a lead.

3.7.4.2.3. Segment Length and Width Test

Another test is used where the great circle length is calculated for the start and end point of the sub-region. The distance divided by the sub-region width (as calculated by area divided by length), and if the length to width ratio is less than 2, the region is flagged (code 101) as a lead with poor confidence.

3.7.4.2.4. Segment Area

The last test will flag (code 56) all sub-regions with area less than 5 km^2 as being too small. The reason the threshold is set to 5 km^2 for this test and 2 km^2 at the test in section 3.7.4.2 is so that the leads rejected for being too small (between 5 km^2 and 2 km^2) will be recorded in a processing log text file; the regions smaller than 2km^2 are not recorded in the log.

3.8. Leads Characterization

A second processing loop is used for lead characterization. The input for this processing is the mask that was described in section 3.7.1. The final product will be a raster mask described in section 4.1 and a text product described in section 4.2.

3.8.1. Region Identification

As in the lead detection process, the label_region function is used to identify and number each region where the detection technique identified a good quality lead (code 100). An erode function is applied to the label mask so that the every 1 km^2 pixel on the edge of each region is removed. The result is a mask that has more disconnected regions than the original mask; these regions are lead branch segments. Each of these smaller branch regions are numbered (via the label_region function) and then via the dilate function the regions are grown back their original size. The branches are processed in a loop.

3.8.2. Lead Branch Processing

The branch processing loop process starts by identifying the remaining branch with the largest area. Similar to the lead identification loop, the characterization loop uses a window centered around the largest remaining lead branch object. If the ratio of branch area divided by length is greater than 60 km^2 then the window is the size of the lead branch, otherwise a 750 km by 750 km window that is centered on the largest remaining lead branch is used. For each processing window, there is a loop to processes each branch (except lead branches that are on the boundary of a search window – they are processed in a window when they are not on the boundary).

3.8.2.1. Lead Branch Edge Calculations

For each lead branch, the edge of the region is defined. This is done by applying the erode function to remove the edge from the region and then subtracting the eroded mask from the original mask. The start and end point of the lead branch is found by finding the set of coordinates that are the furthest distance apart. The great circle distance and azimuth angle are calculated from the start and end points. The segment width is derived by dividing the segment area by great circle length. The region code for start and end points of the branch is recorded to more readily locate leads as a function of region – while noting that some leads may span across region boundaries.

3.8.2.2. Lead Branch Output

After all of the calculations described in section 3.8.2.1, the results are written to an asci file. The file contains a count variable to identify each branch, the start and end coordinates (x, y, longitude, and latitude), length, azimuth, width area, and the region code that corresponds to the start and end point of the branch. Note that lead branches that are only 1km^2 do not have a valid azimuth angle because these are points instead of line segments.

4. Leads Products

The final leads products consist of a raster image showing the location of each processed lead and a text product describing the location of each lead segment.

4.1. Raster Product Description

The derivation of the raster product output is described in section 3.7.4.2. The mask has 1 km resolution and contains the codes described in Table 4.1.

Mask code	Mask Color [R,G,B]	Description
10		Ice concentration threshold not met
50	125,0,125	Too many disconnected sub regions
51	0,0,125	Too symmetric
52	0,125,0	Too circular
53	250,0,250	No good Hough line
55	85,90,115	Cloudy
56	255,128,0	Too small
61	0,255,0	Too wide
62	255,0,0	Preliminary width too wide
100	255,255,255	Lead
101	255,255,0	Low confidence lead; too wide for length

Table 4.1. Mask code descriptions

4.1.1. Raster Product Examples

An example of a raster product image is shown below in Figure 4.1.1. Refer to Table 4.1 for the color code for each mask color.

Figure 4.1.1. Example of lead detection mask from 10 January 2003.

4.2. Text Product Description

The derivation of the text product is described in section 3.8.2.2.

4.2.1. Text Product Examples

An example of text product image is shown below in Table 4.2.1. Refer to section 3.8.2.2 for a description of the fields. For brevity only the first 20 (out of 2626) leads are shown.

count	x_{start}	y_{start}	x_{end}	y_{end}	lon_{start}	lat_{start}	lon_{end}	lat_{end}	length	azimuth	width	area	$region_{start}$	$region_{end}$
	487	366	487	367	157.15	81.65	156.72	81.77						
1	1	0	2	5	1	6	7	7	15.11	153.46	42.41	641	7	7
	483	364	482	366	159.29	81.65	160.06	81.84						
2	9	7	0	3	2	4	0	9	24.97	29.07	20.39	509	7	7
	479	366	477	367	161.42	81.92	162.72	82.09						
3	7	4	2	6	3	6	4	9	27.83	45.65	16.56	461	7	7
	487	370	486	371	155.57	81.99	155.93	82.14						
4	9	4	7	7	2	1	7	3	17.79	18.20	10.45	186	7	7
	487	369	485	371	156.03	81.91	156.63	82.19						
5	6	3	5	8	8	2	6	5	32.84	16.00	4.08	134	7	7
	485	370	485	370	156.89	82.04	156.62	82.10						
6	8	1	9	9	5	3	9	6	8.10	149.89	12.71	103	7	7
	482	370	483	371	158.67	82.18	157.90	82.27						
7	7	5	4	9	8	2	0	7	15.71	132.24	5.67	89	7	7
	489	367	488	368	155.60	81.69	155.70	81.84						
8	2	4	4	8	8	6	3	1	16.23	5.33	4.87	79	7	7
	488	369	488	370	155.14	81.90	154.99	81.97						
9	9	8	8	6	9	4	1	4	8.11	162.36	7.89	64	7	7
	487	367	487	369	156.44	81.77	156.46	81.90						
10	6	7	0	0	6	9	6	9	14.41	1.21	3.82	55	7	7
	492	369	493	370	153.12	81.77	152.36	81.80						
11	4	9	3	8	6	4	2	9	12.75	108.21	4.24	54	7	7
	488	368	487	369	155.98	81.81	156.11	81.88						
12	1	4	6	0	0	9	5	7	7.86	15.71	5.6	44	7	7
	494	371	494	373	151.59	81.84	151.15	81.97						
13	2	7	1	3	2	3	8	4	16.12	155.27	2.42	39	7	7
	480	366	480	367	160.85	81.90	160.83	81.97						
14	6	5	4	2	8	9	2	4	7.33	176.82	4.91	36	7	7
	479	365	480	366	161.78	81.85	161.12	81.88						
15	4	5	3	1	6	8	2	3	10.83	105.55	2.95	32	7	7
	489	364	489	364	156.14	81.45	156.34	81.49						
16	5	6	0	9	2	4	6	7	5.86	35.03	5.46	32	7	7
	489	369	489	370	154.96	81.83	154.92	81.90						
17	5	2	2	0	4	2	1	9	8.60	175.54	3.26	28	7	7
	487	373	487	373	155.25	82.23	154.69	82.27						
18	2	1	8	8	3	9	2	4	9.24	114.75	2.92	27	7	7
	487	366	487	366	157.10	81.67	156.58	81.70						
19	1	2	7	9	3	2	8	9	9.24	116.62	2.81	26	7	7
	487	368	487	368	156.32	81.82	156.36	81.85						
20	6	2	4	5	0	1	0	3	3.63	9.96	7.17	26	7	7

Table 4.2.1. Example text product, first 20 leads from 10 January 2003.

5. Assumptions and Limitations

The algorithm does not perform well along the edge of the sea ice, that is why it has been limited to identifying leads in deep water only. The problem is that it is hard to drawn the distinction between a lead and open water.

Clouds limit detection of leads. Sea ice concentration is not calculated when the cloud mask identifies a cloud. The cloud mask is known to have lower accuracy in polar regions. Cloud and cloud shadows that are not identified by the cloud mask can be misidentified as open water and cause false lead detections. Similarly, open water features can be misidentified as clouds by the cloud mask and are thereby omitted from lead detection. Additionally, leads trends may be difficult to identify due to clouds. Cloud development may be enhanced due to the formation of leads (giving the atmosphere a source of moisture and lift – due to the water being warmer than the neighboring ice and air). And so leads may be becoming more frequent with time, but if cloud cover is also becoming more frequent it would becoming increasingly difficult to detect leads.

This leads detection technique does not take into account ice thickness, therefor the product does not predict neither where leads may likely to develop nor where leads may have previously been (which may be possible with knowledge of where the ice is thin). Similarly, the algorithm does not make an attempt to track leads for either persistence or movement.

6. References

Ackerman, S. A., K. I. Strabala, W. P. Menzel, R. A. Frey, C. C. Moeller, and L. E. Gumley Discriminating Clear-sky from Clouds with MODIS, 1998: *J. Geo. Res*., **103** , D24, p. 32,141

Alam, A. and J. Curry, 1995: Lead-induced atmospheric circulations. *Jour Geo Res*, **100**, C3, 4643-4651.

Appel I., and J. A. Kenneth, 2002: Fresh water ice Visible/Infrared Imager/Radiometer Suite algorithm theoretical basis document, Version 5. SBRS document #: Y2404.

Frey, R. A., S. A. Ackerman, Y. Liu, K. I. Strabala, H. Zhang, J. Key and X. Wang, 2008: Cloud Detection with MODIS, Part I: Recent Improvements in the MODIS Cloud Mask, *JTECH* **25**, 1057-1072.

Hakkinen, S., A. Proshutinsky, and I. Ashik, 2008: Sea ice drift in the Arctic since the 1950s, *Geophys. Res. Lett.*, **35**, L19704, doi:10.1029/2008GL034791, 184

Hall D.K., G.A. Riggs, and V.V. Salomonson, 2001: Algorithm theoretical basis document for the MODIS snow and sea ice mapping algorithms.

Hall D.K., G.A. Riggs, and V.V. Salomonson, 2006: MODIS sea ice products user guide to collection 5.

Key, J., J.A. Maslanik, and E. Ellefsen, 1994: The effects of sensor field-of-view on the geometrical characteristics of sea ice leads and implications for large-area heat flux estimates. *Remote Sensing Environ*., **48**(3), 347-357.

Key, J., R. Stone, J. Maslanik, and E. Ellefsen, 1993: The detectability of sea ice leads in satellite data as a function of atmospheric conditions and measurement scale. *Annals Glaciol*., **17**, 227-232.

Liu Y., and J.R. Key, 2010: Algorithm theoretical basis document for ABI ice cover and concentration. NOAA NESDIS center for satellite applications and research.

Maykut, G. A., 1978: Energy exchange over young sea ice in the central Arctic. *J. Geophys. Res*., **83** (C7), 3646-3658.

Miles, M. W., and R. G. Barry, 1998: A 5-year satellite climatology of winter sea ice leads in the western *Arctic, J. Geophys. Res*., **103**(C10), 21,723–21,734, doi:10.1029/98JC01997.

Murray, R.J., and I. Simmonds, 1995: Responses of climate and cyclones to reductions in Arctic winter sea ice. *J. Geophys. Res*., **100**, 4791-4806.

Smith, S. D., R. D. Muench and C. H. Pease, 1990: Polynyas and leads: An overview of physical processes and environment, J*. Geophys. Res*. **95**, 9461-9470.

Zwally, J., et al., 2002: ICESat's laser measurements of polar ice, atmosphere, ocean and land, *J. Geodyn*., **34**, 405–445.